As a Matter of Tension: Kinetic Energy Spectra in MHD Turbulence

Philipp Grete 10, Brian W. O'Shea 1,2,3 0, and Kris Beckwith 40

1 Department of Physics and Astronomy, Michigan State University, East Lansing, MI:48824, USA; grete@pa.msu.edu.

2 Department of Computational Mathematics, Science and Engineering, Michigan State University, East Lansing, MI:48824, USA

3 National Superconducting Cyclotron Laboratory, Michigan State University, East Lansing, MI:48824, USA

4 Sandia National Laboratories, Albuquerque, NM 87185-1189, USA

Received 2020 September 7; revised 2021 January 11; accepted 2021 January 14; published 2021 March 12

Abstract

While magnetized turbulence is ubiquitous in many astrophysical and terrestrial systems, our understanding of even the simplest physical description of this phenomena, ideal magnetohydrodynamic (MHD) turbulence, remains substantially incomplete. In this work, we highlight the shortcomings of existing theoretical and phenomenological descriptions of MHD turbulence that focus on the joint (kinetic and magnetic) energy fluxes and spectra by demonstrating that treating these quantities separately enables fundamental insights into the dynamics of MHD turbulence. This is accomplished through the analysis of the scale-wise energy transfer over time within an implicit large eddy simulation of subsonic, super-Alfvénic MHD turbulence. Our key finding is that the kinetic energy spectrum develops a scaling of approximately $k^{-4/3}$ in the stationary regime as magnetic tension mediates large-scale kinetic to magnetic energy conversion and significantly suppresses the kinetic energy cascade. This motivates a reevaluation of existing MHD turbulence theories with respect to a more differentiated modeling of the energy fluxes.

Unified Astronomy Thesaurus concepts: Magnetohydrodynamical simulations (1966); Magnetic fields (994); Theoretical techniques (2093); Plasma astrophysics (1261); Magnetohydrodynamics (1964)

Supporting material: tar.gz file

1. Introduction

While our understanding of incompressible hydrodynamic turbulence has significantly advanced over the past decades, many critical questions in the realm of compressible magnetohydrodynamic (MHD) turbulence remain unanswered. This regime is of particular interest in both astrophysics and in terrestrial systems where processes on a huge variety of scales are either governed or at least influenced by MHD turbulence. Astrophysical examples include energy transport in the solar convection zone (Canuto & Christensen-Dalsgaard 1998; Miesch 2005), angular momentum transport and energy release in accretion disks (Balbus & Hawley 1998), the core-collapse supernova mechanism (Couch & Ott 2015; Mösta et al. 2015), the interstellar medium with its star-forming molecular clouds (Falgarone et al. 2015; Vázquez-Semadeni 2015; Klessen & Glover 2016), and clusters of galaxies that can be used to determine cosmological parameters (Brunetti & Jones 2015; Brüggen & Vazza 2015). In the terrestrial context, this is of interest for a range of plasma experiments, such as laserproduced colliding plasma flows, Z-pinches, and tokamaks (see, e.g., Mazzucato et al. 2009; Haines 2011; Ren et al. 2013; Tzeferacos et al. 2018).

At the same time, MHD turbulence theory and phenomenology also made significant progress from early isotropic models (Iroshnikov 1964; Kraichnan 1965), to critically balanced turbulence (Sridhar & Goldreich 1994; Goldreich & Sridhar 1995), to dynamic alignment (Boldyrev 2006), but it is still a highly debated topic—see, e.g., Galtier (2016), Beresnyak (2019), and Verma (2019) for recent reviews. Different theories make a variety of predictions for the scaling of the energy spectra depending on the strength of the mean magnetic field (either external or local), on the cross-helicity (balanced versus unbalanced turbulence), and on the magnetic

helicity (encoding the topology of the magnetic field configuration). In the majority of cases, theoretical scaling predictions are only concerned with the total energy spectrum $(E(k) = E_{kin}(k) + E_{mag}(k)$ with wavenumber k) and assume a moderate or strong background field so that dynamics are differentiated between parallel and perpendicular to the mean field. Thus, in the context of these theories, there is no differentiation between the scaling of kinetic $(E_{kin}(k))$ and magnetic $(E_{\text{mag}}(k))$ energy spectra. A complementary theoretical approach to modeling magnetohydrodynamic turbulence is the use of shell models, which are a computationally inexpensive semianalytical means of modeling turbulence. Notable examples of this include Biskamp (1994), Frick & Sokoloff (1998), and Plunian & Stepanov (2007), who also observe, for example, flatter spectra, spectral breaks, and different scaling behavior of the kinetic and magnetic energy spectra. However, the behavior strongly depends on the characteristics of the system being modeled (with, e.g., the properties of the system such as a mean magnetic field, helicity, and cross-helicity contributing significantly to the observed outcomes, similarly to the locality of the interactions considered). By contrast to predictions from analytic and semianalytic modeling efforts, numerous computational studies of magnetized turbulence have reported different scaling behaviors of kinetic and magnetic energy spectra (Haugen et al. 2004; Aluie & Eyink 2010; Moll et al. 2011; Teaca et al. 2011; Porter et al. 2015; Grete et al. 2017; Bian & Aluie 2019) and, perhaps even more importantly, different scaling behaviors of kinetic and magnetic energy spectra have been reported in observations of the solar wind (Boldyrev et al. 2011).

In order to gain a deeper insight into this discrepancy, we present and analyze the evolution and stationary state of the kinetic and magnetic energy spectra and fluxes separately in the context of an implicit large eddy simulation of ideal MHD

turbulence in its simplest configuration (vanishing mean field, cross-helicity, and magnetic helicity). We confirm prior results (Haugen et al. 2004; Aluie & Eyink 2010; Moll et al. 2011; Teaca et al. 2011; Porter et al. 2015; Grete et al. 2017; Bian & Aluie 2019) that the kinetic and magnetic energy spectra exhibit different scaling behaviors. In particular, we find that the kinetic energy spectrum exhibits a scaling close to $k^{-4/3}$ —i.e., it is shallower than the total energy spectra predicted theoretically, which mostly range between $k^{-3/2}$ and $k^{-5/3}$ (Iroshnikov 1964; Kraichnan 1965; Sridhar & Goldreich 1994; Goldreich & Sridhar 1995; Boldyrev 2006). We further conclude, using a shell-to-shell energy transfer analysis, that this "shallow" kinetic energy spectrum is associated with magnetic tension, which acts to suppress the kinetic energy cascade and provides the major contribution in the energy flux from large to small scales. This result is in marked contrast with incompressible hydrodynamic turbulence, where the conservative kinetic energy cascade is the only means of transferring energy between scales. Under the assumption of self-similarity, Kolmogorov famously showed that this cascade leads to the emergence of a $k^{-5/3}$ scaling in the kinetic energy spectrum (Kolmogorov 1941). However, since then, it has been established that there exist significant departures in the self-similarity giving rise to intermittency (Frisch 1995). Moreover, it has been shown that cascades can also exist for nonconserved quantities, e.g., in compressible hydrodynamic turbulence (Aluie 2011; Aluie et al. 2012) and in incompressible MHD (Bian & Aluie 2019).

Finally, departures from the expected Kolmogorov scaling in hydrodynamic turbulence simulations and experiments have been associated with the existence of "bottlenecks" (Falkovich 1994; Schmidt et al. 2006; Frisch et al. 2008; Donzis & Sreenivasan 2010; Küchler et al. 2019; Agrawal et al. 2020). The results presented in the following demonstrate the rich interactions that can operate even in the simplest MHD scenarios (vanishing mean field, cross-helicity, and magnetic helicity) where magnetic tension is dynamically important. Moreover, the results further serve to highlight the necessary ingredients that MHD turbulence theory and phenomenology should incorporate in order to explain the scalings of kinetic and magnetic energy observed in both simulation and observation of magnetized turbulence.

The rest of this paper is structured as follows. In Section 2, we introduce the simulation setup and summarize the energy transfer analysis. In Section 3, we present the kinetic and magnetic energy spectra, their temporal evolution, and scale-dependent energy dynamics. Finally, in Section 4, we summarize our results, the limitations of the simulations upon which they are based, and discuss the implications for both modeling of magnetohydrodynamic turbulence and astrophysical systems.

2. Method

2.1. Simulation Setup

We use the open-source code, K-Athena(Grete et al. 2021), a performance portable implementation of Athena++ (Stone et al. 2020) based on Kokkos (Edwards et al. 2014), to solve the ideal MHD equations.⁵ The second-order finite

volume scheme employed comprise a Van Leer integrator, constrained transport MHD algorithm, piecewise-linear reconstruction, and Roe Riemann solver (see Stone & Gardiner 2009 for more details on the numerical method). Given that no explicit physical dissipative terms are present, dissipation is purely numerical; as such, the simulations presented here utilize the implicit large eddy simulation (ILES) technique (Grinstein et al. 2007). Turbulent driving is accomplished through a stochastic forcing approach described by Schmidt et al. (2009), implemented within K-Athena using a communication-avoiding algorithm for efficient large-scale parallel simulations on GPUs.

We conduct a single simulation of a cubic domain with a side length of 1 (if not noted, otherwise all units are in code units) and periodic boundary conditions on a 2048^3 grid. The plasma is initially at rest (velocity $\mathbf{u}=0$) with uniform density $(\rho=1)$ and thermal pressure $(p_{\rm th}=1)$. The initial magnetic field configuration $(\mathbf{B}_0=\nabla\times\mathbf{A}_0\text{ with }\mathbf{A}_0=(0,\ 0,\ r_0-r)$ for $r< r_0$ with $r=\sqrt{(x-0.5)^2+(y-0.5)^2}$) is a cylinder with its axis of symmetry in the z-direction and radius $r_0=0.4$ and centered in the xy plane, i.e., there is no magnetic flux going through any of the periodic boundaries. The initial magnetic field strength is comparatively weak, with $\langle E_{\rm mag} \rangle = 0.00125$ corresponding to a plasma beta (ratio of thermal to magnetic pressure) of $\beta_{\rm p}=800$. The plasma is kept approximately isothermal using an adiabatic equation of state with an adiabatic index of $\gamma=1.0001$.

In order to reach a state of stationary turbulence, we employ a large-scale mechanical driving force (having an inverse parabolic shape, $\propto k^2(2k_f - k)^2$, with a peak at $k_f = 2$, where k is the normalized wavenumber). The driving field is purely solenoidal and has an autocorrelation time of 1.0 so that no artificial compressible modes are injected (Grete et al. 2018). In integral the the stationary regime, length $L = \int E_{\rm kin}(k)/kdk/\int E_{\rm kin}(k)dk = 0.32$ (i.e., slightly smaller than the peak forcing scale at 0.5), the rms sonic Mach number is $M_s = 0.54$, the resulting large eddy turnover time is $T = L/(M_s c_s) = 0.59$, the rms Alfvènic Mach number is $M_a = 2.8$, and the mean plasma beta is $\beta_p = 54$.

2.2. Energy Transfer Analysis

For a detailed analysis of the energy dynamics, we apply the shell-to-shell energy transfer analysis presented in Grete et al. (2017), which is an extension of Alexakis et al. (2005) to the compressible regime; see also Dar et al. (2001), Domaradzki et al. (2010), Mininni (2011), Verma (2019), Yang (2019), and references therein. The key idea is to separate energy transfers by their source (some energy budget at some spatial scale Q), sink (some budget at some scale K), and a mediator. Given the isothermal nature of the simulation, we focus on the kinetic and magnetic energy budget only and ignore a detailed analysis of the internal energy budget (see Schmidt & Grete 2019) or non-isothermal statistics (Grete et al. 2020).

In general, the energy transfers are given by

$$\mathcal{T}_{XY}(Q, K)$$
 with $X, Y \in \{U, B\},$ (1)

expressing energy transfer (for T > 0) from shell Q of energy budget X to shell K of energy budget Y. U and B represent the kinetic and magnetic energy budgets, respectively. More

⁵ K-Athena is available at https://gitlab.com/pgrete/kathena. Commit e5faee49 was used to run the simulation, and the parameter file (athinput.fmturb) is contained in the .tar.gz package with this paper.

specifically, the energy transfers are

$$\mathcal{T}_{\text{UU}}(Q, K) = -\int w^{K} \cdot (\boldsymbol{u} \cdot \nabla) w^{Q} + \frac{1}{2} w^{K} \cdot w^{Q} \nabla \cdot \boldsymbol{u} d\boldsymbol{x}, \quad (2)$$

$$\mathcal{T}_{BB}(Q, K) = -\int \mathbf{B}^{K} \cdot (\mathbf{u} \cdot \nabla) \mathbf{B}^{Q} + \frac{1}{2} \mathbf{B}^{K} \cdot \mathbf{B}^{Q} \nabla \cdot \mathbf{u} d\mathbf{x}, \quad (3)$$

for kinetic-to-kinetic (and magnetic-to-magnetic) transfers via advection and compression (typically associated with energy cascades),

$$\mathcal{T}_{\text{BUT}}(Q, K) = \int w^{K} \cdot (v_{A} \cdot \nabla) \boldsymbol{B}^{Q} d\boldsymbol{x}, \tag{4}$$

$$\mathcal{T}_{\text{UBT}}(Q, K) = \int \mathbf{B}^{K} \cdot \nabla \cdot (\mathbf{v}_{A} \otimes \mathbf{w}^{Q}) d\mathbf{x}, \tag{5}$$

for magnetic-to-kinetic (and kinetic-to-magnetic) energy transfer via magnetic tension, and

$$\mathcal{T}_{\text{BUP}}(Q, K) = -\int \frac{\mathbf{w}^{K}}{2\sqrt{\rho}} \cdot \nabla (\mathbf{B} \cdot \mathbf{B}^{Q}) d\mathbf{x}, \tag{6}$$

$$\mathcal{T}_{\text{UBP}}(Q, K) = -\int \mathbf{B}^{K} \cdot \mathbf{B} \nabla \cdot \left(\frac{\mathbf{w}^{Q}}{2\sqrt{\rho}}\right) d\mathbf{x}, \tag{7}$$

for magnetic-to-kinetic (and kinetic-to-magnetic) energy transfer via magnetic pressure. Here, $\mathbf{w} = \sqrt{\rho} \mathbf{u}$ is a mass-weighted velocity chosen so that the spectral kinetic energy density based on $\frac{1}{2}w^2$ is a positive definite quantity (Kida & Orszag 1990) and \mathbf{v}_A is the Alfvén velocity. The velocity \mathbf{w}^K and magnetic field \mathbf{B}^K in a shell K (or Q) are

The velocity w^K and magnetic field B^K in a shell K (or Q) are obtained by a sharp spectral filter in Fourier space with logarithmic spacing. The bounds are given by 1 and $2^{n/4+2}$ for $n \in \{-1, 0, 1, ..., 36\}$. Shells (uppercase, e.g., K) and wavenumbers (lowercase, e.g., K) obey a direct mapping, i.e., K = 24 corresponds to $K \in \{22.6, 26.9\}$.

Given the low sonic Mach number of the simulation (i.e., limited density variations), differences between the shell filtered transfers and transfers obtained through a coarse-graining approach (similar to the formalism employed in large eddy simulations) are expected to be negligible (Aluie 2013; Yang et al. 2016; Zhao & Aluie 2018).

3. Results

3.1. Emergence of a Power Law in $E_{kin}(k)$

In MHD turbulence simulations (independent of numerical method, such as pseudo-spectral DNS, higher-order finite difference, or finite volume ILES) without a strong mean field $(B_0 \ll \langle u \rangle_{\rm RMS})$ and magnetic Prandtl number ${\rm Pm} \approx 1$, two important features emerge in the kinetic and magnetic energy spectra when plotted separately; see Figure 1 for a comparison (Haugen et al. 2004; Aluie & Eyink 2010; Moll et al. 2011; Teaca et al. 2011; Porter et al. 2015; Grete et al. 2017; Bian & Aluie 2019). First, the turbulent dynamo amplifies magnetic fields on all scales, resulting in $E_{\rm mag}(k) > E_{\rm kin}(k)$ on all scales smaller than the forcing scales. Second, the kinetic energy spectrum develops a power-law regime on the magnetically dominated scales with a slope close to -4/3, i.e., shallower than the Kolmogorov slope of -5/3.

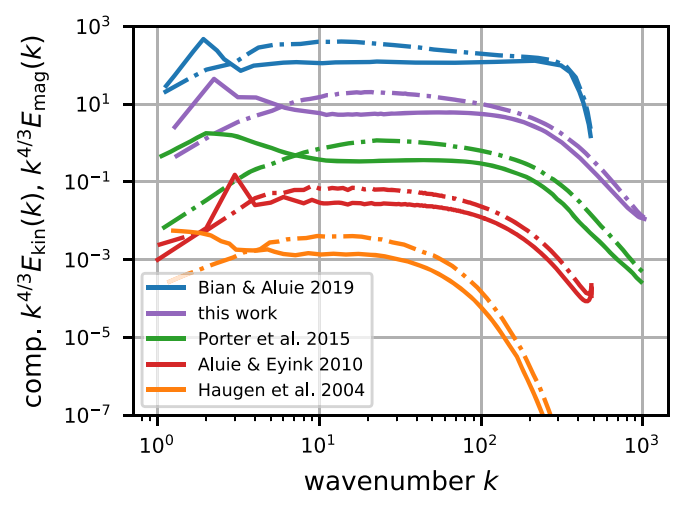


Figure 1. Kinetic (solid) and magnetic (dashed) energy spectra reported in the literature from simulations with various numerical schemes, compensated by $k^{4/3}$: pseudo-spectral DNS of incompressible MHD with hyperdissipation (Bian & Aluie 2019, Figure 8 in their supplementary material), ILES of compressible, ideal MHD (Porter et al. 2015, Figure 3) similar to this work, pseudo-spectral DNS of incompressible MHD (Aluie & Eyink 2010, Figure 1), and higher-order finite difference DNS of compressible MHD with hyperdissipation (Haugen et al. 2004, Figure 7). All spectra have in common that magnetic energy dominates all scales smaller than the forcing scale and that the kinetic energy spectrum exhibits a region with scaling close to $k^{4/3}$. (Lines are vertically offset for increased readability. Data sources: JHTDB for Aluie & Eyink 2010 and original figures using WebPlotDigitizer for other lines.)

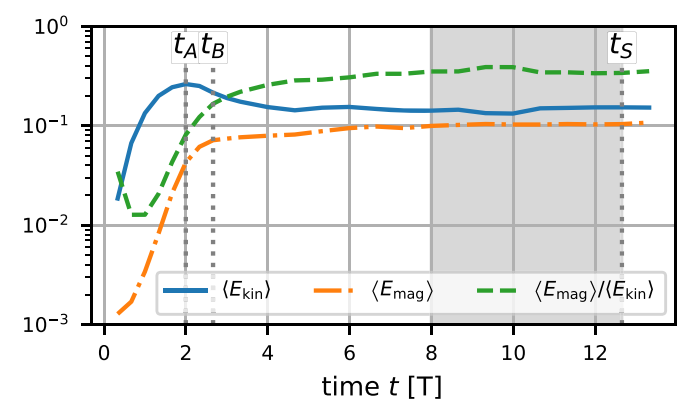


Figure 2. Temporal evolution of the mean magnetic energy (orange dashed-dotted line), mean kinetic energy (blue solid), and their ratio (green dashed). The shaded gray area indicates the stationary regime. Specific times t_A (peak kinetic energy), t_B (nonlinear dynamo), and t_S (stationary) correspond to snapshots that are analyzed in more detail.

We attribute the emergence of a flatter-than-Kolmogorov slope to the effects of magnetic tension and illustrate this conclusion with a detailed analysis of a single simulation in the following sections.

3.2. Time Evolution of the Energy Power Spectra

Figure 2 illustrates the evolution of the mean magnetic and kinetic energies and their ratio over time. First, the mean kinetic energy reaches its peak value at time t_A and roughly marks the transition from the kinetic phase of the turbulent dynamo to the nonlinear phase. The corresponding spectra (top panel in Figure 3) show that the kinetic energy on small

⁶ This decomposition of the energy transfers is not unique; for details and discussion of the physical interpretation, see Grete et al. (2017).

A movie of the temporal evolution of the energy spectra (Grete_et_alspectra_evol.mp4) is available in the .tar.gz package.

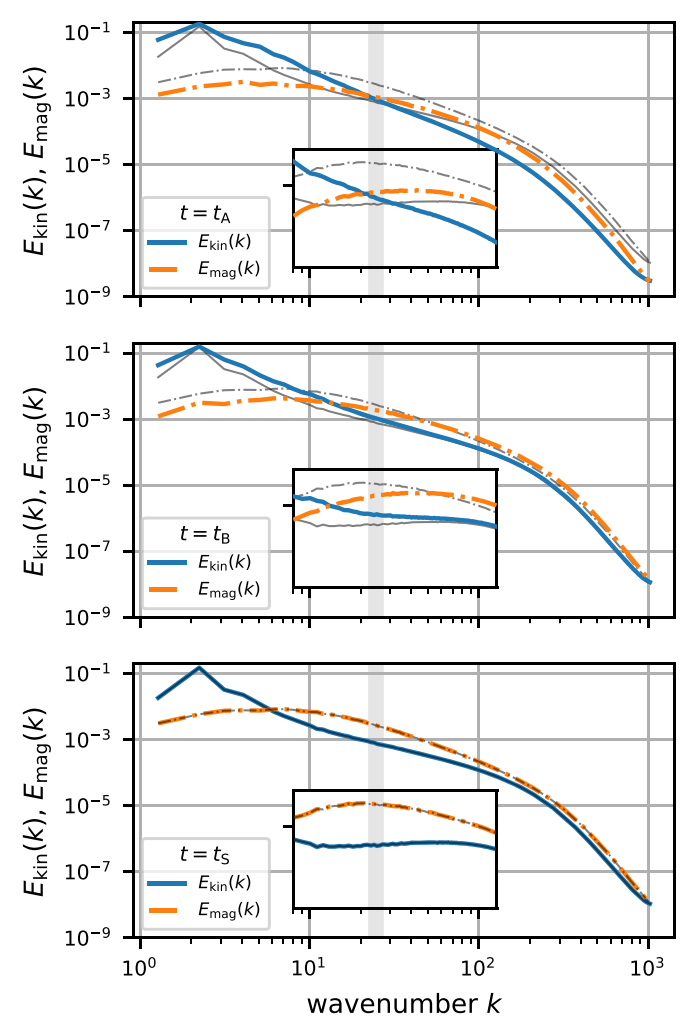


Figure 3. Kinetic (blue solid) and magnetic (orange dashed–dotted) energy spectra at different times. The inset shows 8 < k < 64 compensated by $k^{4/3}$ and illustrates the flattening of the kinetic energy spectrum. The thin black lines in each panel illustrate the stationary state (bottom panel) for reference. The gray area at $22.6 < k \le 26.9$ ($\cong K = 24$) indicates the scale that is used in the more detailed energy transfer analysis in Section 3.3.

scales ($k \gtrsim 32$) is lower than the stationary value (indicated by the thin black lines), whereas the kinetic energy on large scales is above the stationary value. The magnetic energy spectrum crosses the kinetic energy spectrum at $k_{\rm eq} \approx 24$ (where $E_{\rm kin}(k_{\rm eq}) \approx E_{\rm mag}(k_{\rm eq})$) so that the magnetic field becomes dynamically relevant on small scales.

At time t_B , which falls into the nonlinear phase of the dynamo, the kinetic energy on small scales $k \gtrsim 50$ has reached its stationary value (see the center panel in Figure 3). Moreover, the kinetic energy spectrum shows a first indication of a spectral break around $k \approx 24$ with the steeper slope on large scales and a shallower slope on small scales. The crossover of magnetic and kinetic energy has shifted toward larger scales and now occurs around $k_{\rm eq} \approx 16$.

Finally, the stationary regime is reached after $\approx 8T$ with $E_{\rm mag}$ saturating at $\approx 0.28E_{\rm kin}$. In the stationary regime (represented by $t=t_S$), the crossover has shifted to the largest scales $k_{\rm eq}\approx 8$ —see bottom panel of Figure 3. Further growth is inhibited due to the large-scale purely mechanical force, and the magnetic energy is now dominant on all but the largest scales. As a result, the kinetic energy spectrum has been significantly flattened and now exhibits a limited range

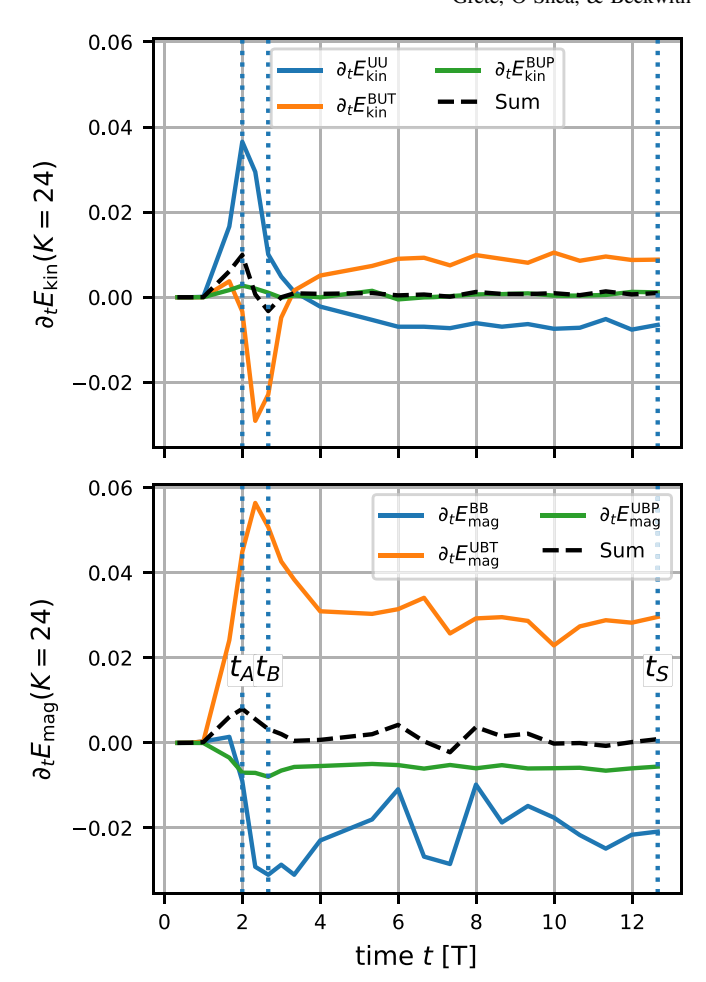


Figure 4. Net rate of change in kinetic (top) and magnetic (bottom) energy at k=24 over time. Blue lines indicate energy transfer through advection, orange through magnetic tension, and green through magnetic pressures. The pressure dilatation and forcing term are not shown as their contribution is negligible.

 $16 \lesssim k \lesssim 64$ with a shallower-than-Kolmogorov slope close to $\approx -4/3$.

In the following, we provide support for the assertion that this flattening of the kinetic energy spectrum is tightly linked to a suppression of the kinetic energy cascade by magnetic tension.

3.3. Energy Dynamics

In the absence of explicit dissipation (and, thus, the explicit mean dissipation rate), all energy transfer rates are normalized using the mean total cross-scale flux at k=26.9 in the stationary regime as a proxy (see Figure 6). This choice has no influence on the actual results but allows for an easier comparison of relative magnitudes and with other results reported in the literature.

3.3.1. Magnetic Tension

The role of magnetic tension in shaping the kinetic energy spectrum becomes apparent in Figure 4. It shows the net rate of change in kinetic energy (top row) and magnetic energy (bottom row for the different mediators over time and for the reference shell K = 24, i.e.,

$$\partial_t E_{\text{kin}}^{XY}(K) = \sum_Q \mathcal{T}_{XY}(Q, K) \text{ and}$$
 (8)

$$\partial_t E_{\text{mag}}^{\text{XY}}(K) = \sum_{\mathcal{Q}} \mathcal{T}_{\text{XY}}(\mathcal{Q}, K),$$
 (9)

with $XY \in \{UU,BUT,BUP\}$ for the kinetic energy and $XY \in \{BB,UBT,UBP\}$ for the magnetic energy. In other words, this is the net rate of change in energy at some scale K from all other scales Q.

While at time t_A the kinetic cascade $(T_{\rm UU})$ is still contributing to a net increase of kinetic energy on those scales, the rate of change by magnetic tension $T_{\rm BUT}$ is negative, i.e., removing kinetic energy from K=24. The net effect remains positive. At t_B , the dynamics have changed. The kinetic cascade still contributes to the growth in kinetic energy, but magnetic tension now dominates so that the net effect is a removal of kinetic energy from those scales. We interpret this transfer of energy from the kinetic to the magnetic budget through magnetic tensions as being tightly related to the flattening of the kinetic energy spectrum.

In the stationary regime, the net rate of change in both kinetic and magnetic energy fluctuates around 0 (otherwise, the regime should not be considered stationary). This balance is only maintained through energy transfers between the kinetic and magnetic energy budgets. On average, the kinetic and magnetic cascades remove energy from intermediate scales of their respective budgets (blue lines are negative), and this deficit is filled through transfers mediated by magnetic tension between budgets (orange lines).

The importance of magnetic tension is similarly observed in the cross-scale energy fluxes. These fluxes are obtained from the individual transport terms via

$$\Pi_{\mathbf{U}^{>}}^{\mathbf{U}^{<}}(k) = \sum_{Q \leqslant k} \sum_{K > k} \mathcal{T}_{\mathbf{U}\mathbf{U}}(Q, K), \tag{10}$$

$$\Pi_{\mathsf{B}^{>}}^{\mathsf{U}^{<},\mathsf{T}}(k) = \sum_{Q \leqslant k} \sum_{K > k} \mathcal{T}_{\mathsf{UBT}}(Q, K),\tag{11}$$

$$\Pi_{\mathsf{B}^{>}}^{\mathsf{U}^{<},\mathsf{P}}(k) = \sum_{Q \leqslant k} \sum_{K > k} \mathcal{T}_{\mathsf{UBP}}(Q, K), \tag{12}$$

for energy being transferred from the kinetic energy on all scales $\leq k$ to the kinetic and magnetic energies on scales smaller than k by advection, magnetic tension, and magnetic pressure, respectively. The same notation applies to transfers from the large-scale magnetic energy with the U and B indices exchanged.

Figure 5 illustrates the energy flux across k = 26.9 over time from the large-scale kinetic energy (top panel) and large-scale magnetic energy (bottom panel). Again, the cross-scale flux initially increases in intensity for both of the advection-related transfers (blue lines). While it peaks for Π_B^{S} at t_B and then remains at a constant value, it already peaks for Π_{U}^{U} at $t = t_A$ and afterward declines again to 0. Transfers via magnetic tension (orange lines) from both large kinetic and magnetic scales steadily grow until $t = t_B$. Similar to the advection transfers, Π_{U}^{S} , T remains constant after the peak, whereas Π_{D}^{U} , T declines, with the key difference that the decline is not to zero but to a nonzero value. Moreover, it is the only remaining contribution for the kinetic energy cross-scale flux (at that scale) and, overall, the dominating cross-scale flux is

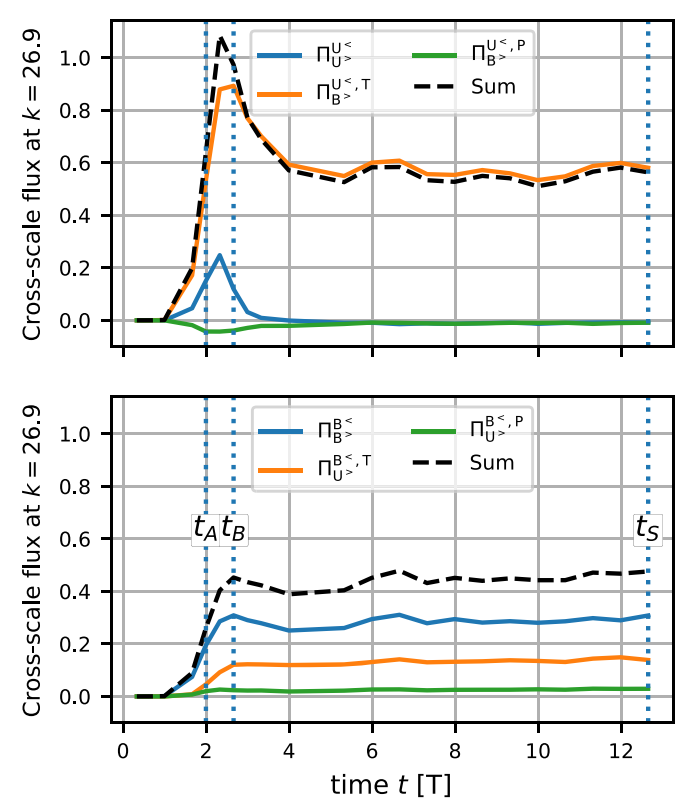


Figure 5. Cross-scale energy transfer across k = 26.9 over time, i.e., the energy from all budgets going from all larger scales (k < 26.9) to the small-scale (k > 26.9) kinetic budget (top) and magnetic budget (bottom), respectively.

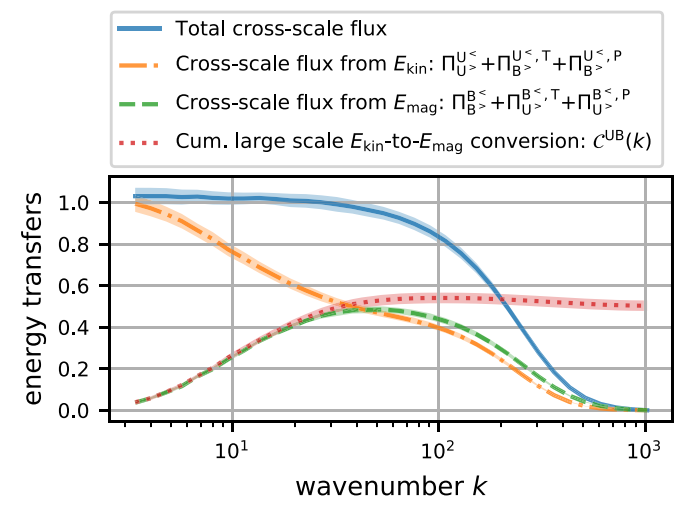


Figure 6. Cross-scale energy transfer across k from the kinetic budget (orange) and magnetic budget (green), and cumulative energy conversion from kinetic to magnetic energy on scales larger than k in the stationary regime.

marginally (\approx 15%–20%) stronger than the combined fluxes from the large-scale magnetic energy budget by advection and tension. In other words, $\Pi_{U^>}^{U^>}$, which is the only cross-scale flux in incompressible hydrodynamics, is completely suppressed here, and the cross-scale energy transfer from the kinetic energy budget is solely mediated by magnetic tension.

3.3.2. Large-scale Energy Conversion

While cross-scale fluxes allow for intra- (via advection) and interbudget (via magnetic tension and pressure) transfers, only

the latter contributes to a conversion of energy between budgets. Figure 6 illustrates the net cross-scale fluxes versus scale in the stationary regime along with the cumulative large-scale kinetic to magnetic energy conversion. The cumulative large-scale conversion refers to the net energy transfer between those two budgets on all scales larger than the reference scale k,

$$C^{\text{UB}}(k) = \sum_{Q,K \leqslant k} \mathcal{T}_{\text{UBT}}(Q,K) + \mathcal{T}_{\text{UBP}}(Q,K), \tag{13}$$

and is analogous to the conversion term introduced in Bian & Aluie (2019) (where the shell-to-shell analysis presented here corresponds to using a sharp spectral kernel in their coarsegraining framework). Note that the magnetic pressure contribution is negligible in the simulation presented here. The cumulative energy conversion tightly follows the cross-scale flux from the magnetic energy budget. On the largest scales $(k \approx 4)$, it is negligible. Here, the cross-scale flux is dominated by the flux from the kinetic energy budget as expected in a situation with a large-scale mechanical driving. From the large to intermediate scales ($k \approx 30$), the contribution continuously grows while the kinetic energy cross-scale flux contribution decreases. Eventually, the kinetic and magnetic cross-scale fluxes become approximately the same strength. Similarly, the cumulative energy conversion reaches a constant value. This implies that no significant net energy conversion occurs on intermediate scales and is in agreement with Bian & Aluie (2019), who analytically and numerically show that mean-field line stretching is a predominantly large-scale process.

4. Summary, Discussion, and Conclusions

Motivated by an apparent discrepancy between kinetic and magnetic energy spectra scalings measured in simulations (Haugen et al. 2004; Aluie & Eyink 2010; Moll et al. 2011; Teaca et al. 2011; Porter et al. 2015; Grete et al. 2017; Bian & Aluie 2019) and observations of the solar wind (Boldyrev et al. 2011) with expectations derived from analytic theory (Galtier 2016; Beresnyak 2019), we presented shell-to-shell energy transfer analysis of an implicit large eddy simulation of approximately isothermal, subsonic, super-Alfvénic MHD turbulence with vanishing background magnetic field, crosshelicity, and magnetic helicity. In the context of this analysis, we find that magnetic tension significantly suppresses the kinetic energy cascade, resulting in a spectrum that is shallower than predicted in various theories, e.g., $E(k) \propto k^{-3/2}$ (Iroshnikov 1964; Kraichnan 1965) or $E(k_{\perp}) \propto k_{\perp}^{-3/2}$ (Boldyrev 2006). Overall, the results presented here indicate that the energy flux across scales is dominated by magnetic tension, and similarly, the scale local energy balance in the stationary turbulence regime is maintained by a constant energy transfer between the kinetic and magnetic reservoirs mediated by magnetic tension.

The simulations on which the results are based are necessarily limited. While a clear signature of an extended range with a scaling close to $k^{-4/3}$ is observed in the kinetic energy power spectrum, no such range is observed in the magnetic energy power spectrum (see Figure 1). We attribute this to a combination of the simulation setup as well as a limited dynamical range. More specifically, the mechanical energy injection on the largest scales provides a barrier for the large-scale magnetic field growth in the absence of a significant (external) mean field. As a result, the magnetic field is strongest

on intermediate scales and gets weaker toward larger scales. Similarly, in the limit of large Reynolds numbers, we expect the ratio of $E_{\rm mag}(k)/E_{\rm kin}(k)$ to grow from the smallest (nondissipative) scales toward larger scales until the growth is inhibited by the forcing acting on the largest scales. This also explains why extended scaling ranges are regularly observed in reduced MHD simulations or in simulations with a significant mean field (potentially stronger than the velocity field on the forcing scales), where it, figuratively, provides a large-scale anchor; see Beresnyak 2019).

In this study, we focus on simulations with magnetic Prandtl numbers of Pm $\simeq 1$ —that is, calculations where the kinetic viscosity and magnetic diffusivity are approximately the same. We note that the results presented here appear to be generally independent of the numerical method in the Pm ≈ 1 regime. As shown in Figure 1, the scaling in the kinetic energy spectrum has been observed in pseudo-spectral, finite difference, and finite volume simulations, and with or without explicit (hyper) dissipative terms. While the relative behavior on the smallest scales will depend on Pm, overall, it is expected that for Rm > Re (i.e., Pm > 1), where magnetic diffusivity is very low compared to kinetic viscosity, magnetic energy will be amplified above the kinetic energy on all scales smaller than the energy injection scale, with the opposite effect happening in the Pm < 1 regime (Brandenburg 2014). While shell models suggest that the magnetic field will continue to show the behavior we have observed in the Pm $\gg 1$ regime, at Pm $\ll 1$ (i.e., when the magnetic diffusion rate is high), it is likely that there will be very little magnetic power at small scales, although the precise details will likely depend on the nature of the turbulent driving. Given that a wide range of magnetic Prandtl numbers are relevant in both terrestrial and astrophysical systems, further work exploring a wider range of Pm is well motivated.

Further complexity arises when we consider variations in the plasma regime. We are modeling a plasma using the ideal MHD approximation—i.e., assuming that particles are highly collisional, that the Debye length and electron and ion gyroradii are small, and that the inverse of the electron and ion cyclotron frequencies are short compared to the spatial and temporal scales of interest. As these assumptions are relaxed—for example, if the plasma is assumed to be weakly collisional and thus viscosity and resistivity become significantly anisotropic —this may impact the results we have observed. Such regimes are important for both terrestrial and astrophysical systems, and while they are beyond the scope of our current efforts, they are worthy of consideration. This may require a substantially different numerical approach, however. While some deviations from the ideal MHD regime can be explored with extensions of the MHD approximation (e.g., adding anisotropic terms as per the Braginskii approximation; Braginskii 1965), it is likely that a kinetic or hybrid fluid/kinetic approximation will be required for some physical regimes.

The key finding of this work is that magnetic tension acts to suppress cross-scale kinetic energy transfer, resulting in a kinetic spectrum with a slope $k^{-4/3}$, in contrast with theoretical expectations regarding incompressible hydrodynamic turbulence. Such a suppression of cross-scale kinetic energy transfer is also observed in simulations of hydrodynamics turbulence, where the "bottleneck effect" (a pileup of energy on the smallest scales) results in a shallower than $k^{-5/3}$ scaling in the kinetic energy spectrum in hydrodynamic turbulence

(Falkovich 1994; Schmidt et al. 2006; Frisch et al. 2008; Donzis & Sreenivasan 2010; Küchler et al. 2019; Agrawal et al. 2020). Recently, Gong et al. (2020) also attributed the hydrodynamic bottleneck effect to the shallow kinetic energy spectra they observe in their MHD simulations.

The results presented here demonstrate that, contrary to Gong et al. (2020), the physical mechanism for the shallow slope of the kinetic energy spectrum is fundamentally different between hydrodynamics and magnetohydrodynamics due to magnetic tension (which is naturally absent in hydrodynamics). In addition, the results presented here suggest that the kinetic cascade, $\Pi_{\Pi^{>}}^{U^{<}}$, is practically absent on intermediate scales in the analyzed simulation. This is in agreement with Brandenburg & Rempel (2019), who find, in a comparable $Pm \approx 1$ regime, that the main energy flow follows a path from large-scale kinetic to large-scale magnetic energy, followed by large magnetic to small-scale magnetic, and eventually small-scale magnetic to small-scale kinetic energy. The large-scale energy conversion is also in agreement with Bian & Aluie (2019), as detailed in Section 3.3.2. However, the strongly suppressed kinetic cascade we see in the simulation differs from the decoupled cascade theory on intermediate scales brought forward by Bian & Aluie (2019). While we still observe a significant energy flux in the magnetic energy cascade, the balance in the kinetic energy budget is maintained by magnetic tension. Thus, both energy budgets remain coupled through dynamically significant energy fluxes. Note, compared to the vastly extended dynamical range in Bian & Aluie (2019; which comes from the use of higher-order hyperdissipative terms), the dynamical range in the simulation presented here is rather limited. While the simulation presented here may not reach an (extended) decoupled regime, Bian & Aluie (2019) also observe an approximately $k^{-4/3}$ scaling across the conversion and decoupled scales; see Figure 1. Moreover, the ILES nature of our simulation precludes an exact analysis of the dissipative scales. Future simulations with a larger dynamical range and explicit viscosity and resistivity will help to address the conundrum between suppressed and coupled cascades.

With these caveats in mind, the results presented here have a number of implications. First, they motivate a reevaluation of MHD turbulence theories that commonly are only concerned with the total (kinetic and magnetic) energy spectrum and energy flux. In particular, the results presented here suggest that flux-based models should differentiate between the intra- and interbudget cross-scale fluxes, and consider energy budgets separately. We note that the scaling of the total energy will be dominated by the magnetic energy scaling on intermediate scales, which is important in light of MHD turbulence theory on scaling relations. Second, in the interpretation of observations and their derived spectra, special care is required in inferring properties from one spectrum to another, as we see no indication that kinetic and magnetic energy spectra follow the same scaling laws, (see also Boldyrev et al. 2011). Third, subgrid-scale modeling in the context of large eddy simulations (Miesch et al. 2015; Grete et al. 2016) may become simpler as, for example, one can ignore a purely kinetic cross-scale flux. Finally, we note that in natural systems the effective, largescale driving mechanisms, e.g., a galaxy cluster merger (Subramanian et al. 2006), provide an outer scale and limit for the amplification of magnetic fields by the fluctuation dynamo.

Finally, we note that the results presented here should also be interpreted with care and not be overgeneralized. As mentioned in the Introduction, the configuration space of MHD turbulence is vast and this work covers only a single point. Additional data from (even larger-scale) simulations, observations, and experiments are required in order to get a complete picture of MHD turbulence.

The authors thank Jim Stone and Ellen Zweibel for useful discussions. P.G. and B.W.O. acknowledge funding by NASA Astrophysics Theory Program grant #NNX15AP39G. Sandia National Laboratories is a multimission laboratory managed and operated by National Technology and Engineering Solutions of Sandia LLC, a wholly owned subsidiary of Honeywell International Inc., for the US Department of Energy's National Nuclear Security Administration under contract DE-NA0003525. The views expressed in the article do not necessarily represent the views of the US Department of Energy or the United States Government. SAND Number: SAND2021-1232 J. B.W.O. acknowledges additional funding by NSF grants #1514700, AST-1517908, and AST-1908109, and NASA ATP grant 80NSSC18K1105.

The simulations and analysis were run on the NASA Pleiades supercomputer through allocation SMD-16-7720, on TACC's Stampede2 supercomputer as part of the Extreme Science and Engineering Discovery Environment (XSEDE Towns et al. 2014), which is supported by National Science Foundation grant number ACI-1548562, through allocation #TG-AST090040, and on TACC's Frontera supercomputer through LRAC allocation #AST20004 funded by NSF grant 1818253.

The software below is developed by a large number of independent researchers from numerous institutions around the world. Their commitment to open science has helped make this work possible.

Software: K-Athena (Grete et al. 2021), a performance portable version of Athena++ (Stone et al. 2020) using Kokkos (Edwards et al. 2014), WebPlotDigitizer (Rohatgi 2020), Matplotlib (Hunter 2007), NumPy (van der Walt et al. 2011), mpi4py (Dalcín et al. 2005), mpi4py-fft (Dalcin et al. 2019).

ORCID iDs

Philipp Grete https://orcid.org/0000-0003-3555-9886
Brian W. O'Shea https://orcid.org/0000-0002-2786-0348
Kris Beckwith https://orcid.org/0000-0002-5610-8331

References

```
Agrawal, R., Alexakis, A., Brachet, M. E., & Tuckerman, L. S. 2020, PhRvF,
  5, 024601
Alexakis, A., Mininni, P. D., & Pouquet, A. 2005, PhRvE, 72, 046301
Aluie, H. 2011, PhRvL, 106, 174502
Aluie, H. 2013, PhyD, 247, 54
Aluie, H., & Eyink, G. L. 2010, PhRvL, 104, 081101
Aluie, H., Li, S., & Li, H. 2012, ApJ, 751, L29
Balbus, S. A., & Hawley, J. F. 1998, RvMP, 70, 1
Beresnyak, A. 2019, LRCA, 5, 2
Bian, X., & Aluie, H. 2019, PhRvL, 122, 135101
Biskamp, D. 1994, PhRvE, 50, 2702
Boldyrev, S. 2006, PhRvL, 96, 115002
Boldyrev, S., Perez, J. C., Borovsky, J. E., & Podesta, J. J. 2011, ApJ, 741, L19
Braginskii, S. I. 1965, RvPP, 1, 205
Brandenburg, A. 2014, ApJ, 791, 12
Brandenburg, A., & Rempel, M. 2019, ApJ, 879, 57
```

```
Brüggen, M., & Vazza, F. 2015, in Turbulence in the Intracluster Medium, ed. A. Lazarian et al. (Berlin: Springer), 599

Brugetti, G., & Janes, T. W. 2015, in Compic Reve in Golavy, Chapters, and
```

Brunetti, G., & Jones, T. W. 2015, in Cosmic Rays in Galaxy Clusters and Their Interaction with Magnetic Fields, ed. A. Lazarian et al. (Berlin: Springer), 557

Canuto, V. M., & Christensen-Dalsgaard, J. 1998, AnRFM, 30, 167

Couch, S. M., & Ott, C. D. 2015, ApJ, 799, 5

Dalcin, L., Mortensen, M., & Keyes, D. E. 2019, JPDC, 128, 137

Dalcín, L., Paz, R., & Storti, M. 2005, JPDC, 65, 1108

Dar, G., Verma, M. K., & Eswaran, V. 2001, PhyD, 157, 207

Domaradzki, J. A., Teaca, B., & Carati, D. 2010, PhFl, 22, 051702

Donzis, D. A., & Sreenivasan, K. R. 2010, JFM, 657, 171

Edwards, H. C., Trott, C. R., & Sunderland, D. 2014, JPDC, 74, 3202

Falgarone, E., Momferratos, G., & Lesaffre, P. 2015, in The Intermittency of ISM Turbulence: What Do the Observations Tell Us?, ed. A. Lazarian et al. (Berlin: Springer), 227

Falkovich, G. 1994, PhFl, 6, 1411

Frick, P., & Sokoloff, D. 1998, PhRvE, 57, 4155

Frisch, U. 1995, Turbulence: The Legacy of AN Kolmogorov (Cambridge: Cambridge Univ. Press)

Frisch, U., Kurien, S., Pandit, R., et al. 2008, PhRvL, 101, 144501

Galtier, S. 2016, Introduction to Modern Magnetohydrodynamics (Cambridge: Cambridge Univ. Press)

Goldreich, P., & Sridhar, S. 1995, ApJ, 438, 763

Gong, M., Ivlev, A. V., Zhao, B., & Caselli, P. 2020, ApJ, 891, 172

Grete, P., Glines, F. W., & O'Shea, B. W. 2021, IEEE Trans. on Parallel and Distributed Systems, Vol. 32 (Piscataway, NJ: IEEE), 85

Grete, P., O'Shea, B. W., & Beckwith, K. 2018, ApJL, 858, L19

Grete, P., O'Shea, B. W., & Beckwith, K. 2020, ApJ, 889, 19

Grete, P., O'Shea, B. W., Beckwith, K., Schmidt, W., & Christlieb, A. 2017, PhPl, 24, 092311

Grete, P., Vlaykov, D. G., Schmidt, W., & Schleicher, D. R. G. 2016, PhPl, 23, 062317

Grinstein, F., Margolin, L., & Rider, W. 2007, Implicit Large Eddy Simulation: Computing Turbulent Fluid Dynamics (Cambridge: Cambridge Univ. Press).

Haines, M. G. 2011, PPCF, 53, 093001

Haugen, N. E. L., Brandenburg, A., & Dobler, W. 2004, PhRvE, 70, 016308 Hunter, J. D. 2007, CSE, 9, 90

Iroshnikov, P. S. 1964, SvA, 7, 566

```
Kida, S., & Orszag, S. A. 1990, JSCom, 5, 85
```

Klessen, R. S., & Glover, S. C. 2016, in Saas-Fee Advanced Course, Vol. 43, Star Formation in Galaxy Evolution: Connecting Numerical Models to Reality, ed. Y. Revaz (Berlin: Springer), 85

Kolmogorov, A. 1941, DoSSR, 30, 301

Kraichnan, R. H. 1965, PhFl, 8, 1385

Küchler, C., Bewley, G., & Bodenschatz, E. 2019, JSP, 175, 617

Mazzucato, E., Bell, R. E., Ethier, S., et al. 2009, NucFu, 49, 055001

Missch, M., Matthaeus, W., Brandenburg, A., et al. 2015, SSRv, 194, 97

Miesch, M. S. 2005, LRSP, 2, 139

Mininni, P. D. 2011, AnRFM, 43, 377

Moll, R., Graham, J. P., Pratt, J., et al. 2011, ApJ, 736, 36

Mösta, P., Ott, C. D., Radice, D., et al. 2015, Natur, 528, 376

Plunian, F., & Stepanov, R. 2007, NJPh, 9, 294

Porter, D. H., Jones, T. W., & Ryu, D. 2015, ApJ, 810, 93

Ren, Y., Guttenfelder, W., Kaye, S. M., et al. 2013, NucFu, 53, 083007

Rohatgi, A. 2020, Webplotdigitizer: Version 4.3., https://automeris.io/ WebPlotDigitizer

Schmidt, W., Federrath, C., Hupp, M., Kern, S., & Niemeyer, J. C. 2009, A&A, 494, 127

Schmidt, W., & Grete, P. 2019, PhRvE, 100, 043116

Schmidt, W., Hillebrandt, W., & Niemeyer, J. C. 2006, Comput. Fluids, 35, 353

Sridhar, S., & Goldreich, P. 1994, ApJ, 432, 612

Stone, J. M., & Gardiner, T. 2009, NewA, 14, 139

Stone, J. M., Tomida, K., White, C. J., & Felker, K. G. 2020, ApJS, 249, 4 Subramanian, K., Shukurov, A., & Haugen, N. E. L. 2006, MNRAS, 366, 1437

Teaca, B., Carati, D., & Domaradzki, J. A. 2011, PhPl, 18, 112307

Towns, J., Cockerill, T., Dahan, M., et al. 2014, CSE, 16, 62

Tzeferacos, P., Rigby, A., Bott, A. F. A., et al. 2018, NatCo, 9, 591

van der Walt, S., Colbert, S. C., & Varoquaux, G. 2011, CSE, 13, 22

Vázquez-Semadeni, E. 2015, in Interstellar MHD Turbulence and Star Formation, ed. A. Lazarian et al. (Berlin: Springer), 401

Verma, M. K. 2019, Energy Transfers in Fluid Flows: Multiscale and Spectral Perspectives (Cambridge: Cambridge Univ. Press),

Yang, Y. 2019, Energy Cascade in Compressible MHD Turbulence (Singapore: Springer), 69

Yang, Y., Shi, Y., Wan, M., Matthaeus, W. H., & Chen, S. 2016, PhRvE, 93, 061102

Zhao, D., & Aluie, H. 2018, PhRvF, 3, 054603